primary vortex. As expected, increase/decrease of the feeding rate of the shear-layer vorticity leads directly to the enhancing/weakening of the primary vortex, respectively. Vorticity from the secondary vortex can be carried into the primary vortex as indicated by the presence of low-level counterclockwise vorticity in the primary vortex in the original PIV data. However, the entrained counterclockwise vorticity is relatively weak compared to the primary vorticity so it has not shown up in the interpolated vorticity data. Nevertheless, it can still play a role in weakening the primary vortex as suggested by Gordnier and Visbal[14] in their computational work.

#### Weakening of Both the Primary and the Secondary Vortices

The secondary vortex is significantly weakened after part of its vorticity is ejected from the surface. On the other hand, the weakening of the primary vortex results in the weakening of outboard-moving boundary-layer flow and this consequently hinders the recovery of the secondary vortex. In other words, one would expect that the feeding of vorticity into the secondary vortex would be related to the instantaneous variation of the total circulation of the primary vortex. Time variations of the circulation of the primary vortex and the vorticity flux of the secondary vortex are found to be strongly correlated (not shown here).

#### Reconnection of the Primary Vortex and the Shear Layer

The weakening of the primary vortex implies a smaller induction force on the secondary vortex. As a result, the secondary vortex settles back to the surface. In addition, the secondary vortex reduces in size and strength because of its ejection. The reduced influence of the secondary vortex allows the reconnection of the shear layer with the primary vortex, which in turn resumes the feeding of the shear-layer vorticity into the primary vortex. This event reenergizes the primary vortex, and a new cycle of the primary/secondary vortex interaction repeats.

It is clear from the preceding discussions that the primary/secondary vortex interaction process assumes a self-sustained manner. Once it is initiated, this interaction process no longer requires external perturbations to sustain it. At present, the exact triggering source for our experiments is not clear, although we suspect that inherent disturbances from the experimental setup (the vibration of the water towing tank facility) might be responsible, as another study[15] has suggested. Hubner and Komerath[16] have studied the quasi-periodic velocity fluctuations over a delta wing and showed the existence of fluctuating energy within a narrow frequency bandwidth. They further showed that the quasi-periodicity originated in the outboard region along the leading edge of the wing. This is consistent with the current observation that the interaction between the primary vortex and the secondary vortex occurs outboard near the leading edge.

Even in the absence of any inherent disturbances from the experimental setup, such ejection phenomenon has been observed in a numerical study.[5] Because the interaction is essentially self-sustained, it does not require any external excitations once it is initiated. Therefore, the interaction process can be considered as inherent and can be activated by many potential sources, such as the vibrations of the experimental setup, the interaction between the two primary vortices, the freestream and/or shear-layer disturbances, and the onset of vortex breakdown and wake instabilities.

## Summary

The emphasis of our study is on understanding the vorticity dynamics and the unsteady characteristics of the delta-wing leading-edge vortices. Measurements taken on the crossflow planes reveal a self-sustained, quasi-periodic oscillation of the vortex system. Detailed analysis shows that the process is a direct result of a strong interaction between the primary vortex and the secondary vortex.

## References

[1]Hall, M. G., "Vortex Breakdown," *Annual Review of Fluid Mechanics*, Vol. 4, 1972, pp. 195–218.

[2]Leibovich, S., "The Structure of Vortex Breakdown," *Annual Review of Fluid Mechanics*, Vol. 10, 1978, pp. 221–246.

[3]Escudier, M., "Vortex Breakdown: Observations and Explanations," *Progress in Aerospace Science*, Vol. 25, No. 2, 1988, pp. 189–229.

[4]Riley, A. J., and Lowson, M. V., "Development of a Three-Dimensional Free Shear Layer," *Journal of Fluid Mechanics*, Vol. 369, 1998, pp. 49–89.

[5]Cipolla, K. M., and Rockwell, D., "Small-Scale Vortical Structures in Crossflow Plane of a Rolling Delta Wing," *AIAA Journal*, Vol. 36, No. 12, 1998, pp. 2276–2278.

[6]Gursul, I., and Xie, W. S., "Buffeting Flows over Delta Wings," *AIAA Journal*, Vol. 37, No. 1, 1999, pp. 58–65.

[7]Ozgoren, M., Sahin, B., and Rockwell, D., "Vortex Structure on a Delta Wing at High Angle of Attack," *AIAA Journal*, Vol. 40, No. 2, 2002, pp. 285–292.

[8]Shih, C., and Ding, Z., "Unsteady Structure of Leading-Edge Vortex Flow over a Delta Wing," AIAA Paper 96-0664, Jan. 1996.

[9]Lin, J.-C., and Rockwell, D., "Transient Structure of Vortex Breakdown on a Delta Wing at High Angles of Attack," *AIAA Journal*, Vol. 33, No. 1, 1995, pp. 6–12.

[10]Visbal, M. R., "Origin of Computed Unsteadiness in the Shear Layer of Delta Wings," *Journal of Aircraft*, Vol. 32, No. 5, 1995, pp. 1146, 1147.

[11]Visbal, M. R., "Computational and Physical Aspects of Vortex Breakdown on Delta Wings," AIAA Paper 95-0585, Jan. 1995.

[12]Lourenco, L. M., Krothapalli, A., and Smith, C. A., "Particle Image Velocimeter," *Lecture Notes in Engineering*, edited by M. Gad-el-Hak, Vol. 45, Springer-Verlag, New York, 1989, pp. 127–199.

[13]Adrian, R. J., "Particle-Imaging Techniques for Experimental Fluid Mechanics," *Annual Review of Fluid Mechanics*, Vol. 23, 1991, pp. 261–304.

[14]Gordnier, R. E., and Visbal, M. R., "Unsteady Vortex Structure over a Delta Wing," *Journal of Aircraft*, Vol. 31, No. 1, 1994, pp. 243–248.

[15]Washburn, A. E., and Visser, K. D., "Evolution of Vortical Structures in the Shear Layer of Delta Wings," AIAA Paper 94-2317, June 1994.

[16]Hubner, J. P., and Komerath, N. M., "Spectral Mapping of Quasiperiodic Structures in a Vortex Flow," *Journal of Aircraft*, Vol. 32, No. 3, 1995, pp. 493–500.

J. C. Hermanson
*Associate Editor*

# Numerical Study of N-Wave Propagation Using Optimized Compact Finite Difference Schemes

In Bo Shim,* Jae Wook Kim,† and Duck Joo Lee‡
*Korea Advanced Institute of Science and Technology, Daejeon 305-701, Republic of Korea*

## Introduction

AMONG the aircraft noise sources, the fan is a dominant one in the high-bypass engine, especially during takeoff and landing. The fan noise can be classified into three types: blade passage frequency (BPF) tonal noise, multiple pure tonal (MPT) noise, and broadband noise. MPT noise levels can exceed the BPF tonal noise during takeoff and landing because shock waves are generated at the rotor tip in the today's high-bypass engine when the revolutions per minute of the engine shaft is increased to get maximum thrust.

Hawkings[1] analyzed the shock wave coalescence by using one-dimensional saw-toothed shock models. His analysis describes how an initial nonuniform wave train evolves to become increasingly irregular with distance. However, this type of analysis cannot be directly related to the irregularities in the fan geometry. The drawback

Received 21 March 2002; revision received 30 September 2002; accepted for publication 31 October 2002. 

*Graduate Student, Department of Aerospace Engineering, 373-1 Kuseong-dong, Yuseong-gu; ibshim@acoustic.kaist.ac.kr.

†BK21 Research Professor, Department of Aerospace Engineering, 373-1 Kuseong-dong, Yuseong-gu; jwkim@acoustic.kaist.ac.kr.

‡Professor, Department of Aerospace Engineering, 373-1 Kuseong-dong, Yuseong-gu; djlee@mail.kaist.ac.kr. Member AIAA.

was overcome by Kurosaka,[2] who used the method of characteristics and the oblique shock relations to carry out two-dimensional analysis. He showed that the errors in blade stagger are much more important for producing the multiple pure tones than those in blade spacing. Fisher et al.[3] extended previous considerations of buzz-saw noise propagation in hard-walled ducts to a more practical case of ducts containing acoustic liners for regular and irregular N waves. Recently, McApline and Fisher[4] predicted MPT noise propagation with hard or soft wall using time-domain numerical solution and Frequency-domain numerical solution models based on weak shock theory.

The major objective of this Note is to study this N-wave propagation by using high-order and high-resolution numerical schemes for computational aeroacoustics (CAA) and to compare the numerical solutions with the theoretical results. The suitable number of grid points per wavelength (PPW) for the N wave is investigated.

## Governing Equations and Numerical Methods

Time-dependent one-dimensional Euler equations that are represented as $\partial \boldsymbol{Q}/\partial t + \partial \boldsymbol{E}/\partial t = 0$, where $\boldsymbol{Q} = [\rho, \rho u, \rho e_t]^T$ and $\boldsymbol{E} = [\rho u, \rho u^2 + p, (\rho e_t + p)u]^T$, are used for the computation of the nonlinear wave propagations. The variables $\rho$, $u$, $p$, and $e_t$ are the density, velocity, pressure, and total energy, respectively. The pressure $p$ is related to other variables by $p = (\gamma - 1)(\rho e_t - \rho u^2/2)$, where $\gamma$ is the ratio of specific heats.

The main scheme is a pentadiagonal type of central compact finite difference scheme.[5] This scheme is optimized to achieve maximum resolution characteristics with fourth-order accuracy. The classical fourth-order Runge–Kutta scheme is used for high-order time integration of the solutions. High-order schemes in space and time resolve a wider range of wave number or frequencies than low-order methods. However, even the present schemes do not resolve the highest wave number or frequency range effectively; hence, an adaptive nonlinear artificial dissipation (ANAD)[6] model is also used to remove the unwanted numerical oscillations that may develop from the unresolved frequency range.

## Numerical Results and Discussion

This section presents the results of calculation in three different problems: oscillating piston, regular N-wave propagation, and irregular N-wave propagation. The first two problems are used for verifying the accuracy of the numerical schemes in four different cases of grid numbers, 12.5, 25, 50, and 100 PPW. The last one is solved as a test problem to investigate the feasibility of the present approach for simulating the irregularity of the MPT noise.

### A. Oscillating Piston Problem

The one-dimensional propagation of plane wave is an appropriate model problem to test numerical schemes for calculating nonlinear N waves. This problem, shown in Fig. 1, has a piston that begins to oscillate sinusoidally to form a wave train. The initial waves propagate essentially in a linear manner but gradually steepen and eventually form shocks. For low-amplitude waves, Whitham[7] developed an analytical solution that is suitable for direct comparison with the numerical solutions.

The amplitude of piston velocity $u_p/a_0$ is 0.025, and frequency $\omega_p \lambda/a_0$ is $2\pi$, where $a_0$ is the ambient speed of sound and $\lambda$ is the wavelength. The density and pressure on the piston are calculated by solving the governing equations with characteristic treatment.[8] Figure 1 shows the comparison of the numerical and the analytical solutions. The more grid points that are used, the better are solutions that are obtained. However, there is an overshoot in the vicinity of discontinuity for the high-PPW case. The present numerical methods give a reasonable solution when 25 PPW is used in the computation. Figure 2 shows the Fourier transform of the pressure signal at $x/\lambda = 20$ for each PPW. As shown in Fig. 2, the seventh harmonic can be resolved with 50 PPW and the third harmonic with 25 PPW. If the PPW is lower than 25, then the resolution is very poor, and it is hard to capture the N wave that is composed of many sinusoidal waves.

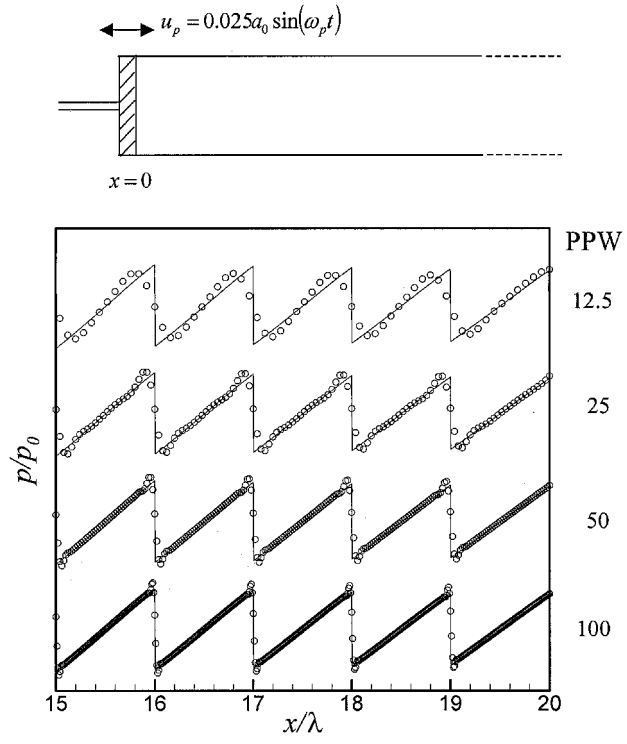


**Fig. 1 Comparison of numerical solutions with analytical solution of piston problem: ○, numerical solution and ——, analytical solution.**

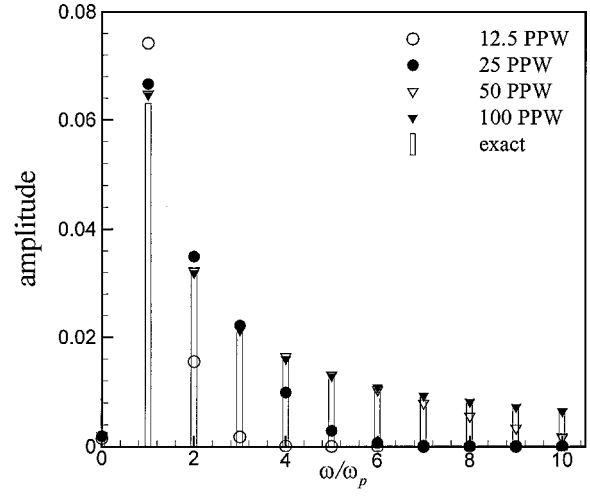


**Fig. 2 Fourier transforms of pressure signal at $x/\lambda = 20$.**

### B. Regular N-Wave Propagation

Fisher et al.[3] did an early idealization of regular N-wave propagation process, and the essentials of the process are summarized as follows. Because of the high amplitude, each point on the expansion fan travels, relative to the fluid, at a velocity as a function of pressure difference $\Delta p$: $v(\Delta p) = a_0 + (\gamma + 1)\Delta p/(2\rho_0 a_0)$, where $\Delta p$ is the deviation from the ambient static pressure $p_0$, $\gamma$ is the specific heat ratio of the fluid, and $\rho_0$ is the ambient density. The shock wave is assumed to travel at the arithmetic average of the velocities, and the wavelength $\lambda$ and the shape of the N wave are maintained. The interaction between the associated shock wave/expansion fan yields the decreasing amplitude as a function of time, which was shown by Fisher et al.[3] The resulting equation is given by

$$p_s(t) = \frac{p_0 s}{1 + [(\gamma + 1)/2\gamma](a_0 t/\lambda)s} \tag{1}$$

where $p_s$ is the amplitude of shock and $s = p_s(0)/p_0$ is the nondimensional starting shock strength. Equation (1) is used for comparison with the numerical solutions.

The density, velocity, and pressure are directly specified at the boundary point $x = 0$ by the N-wave profiles, rather than sinusoidally pulsated by the piston as used in the preceding problem. In Fig. 3, there are comparisons of the numerical solutions with Eq. (1). If at least 25 PPW are used, the numerical solution shows a good agreement with the theoretical solution.

### C. Irregular N-Wave Propagation

Regular N-wave analysis can provide useful estimates of buzz-saw noise propagation, but it lacks an essential element of the actual N-wave phenomena. That is the shock coalescence phenomenon. Because of the nonuniform blade geometry and spacing, slightly different shock waves are produced. Higher amplitude N waves move faster than lower amplitude waves, and so shock coalescence occurs. The position of the shock coalescence and the shock strength can be obtained as follows.[3]

Consider two adjacent shock waves whose difference of shock pressures at the midpoint is $\Delta p_m$. The difference in their translational velocities is, therefore, $\Delta v = \Delta p_m(\gamma + 1)/(2\rho_0 a_0)$. If they were initially a distance $\lambda$ apart, coalescence will occur when $t_c = \lambda/\Delta v$. Substitution of the earlier value of $\Delta v$, together with the use of the relationship $a_0^2 = \gamma p_0/\rho_0$ then yields

$$a_0 t_c/\lambda = [2\gamma/(\gamma + 1)](p_0/\Delta p_m) \tag{2}$$

Equation (2) is used for validating the numerical calculation of the shock coalescence phenomenon. The initial waveform for the numerical calculation is given in Fig. 4, where the third and the fourth N waves are irregular ($\Delta p_m = p_0 s/2$). The shock strength factor is given by $s = 0.1$. From Eq. (2), the time of the first shock coalescence is expected is

$$t_c^* = t_c(a_0/\lambda) = 4\gamma/(\gamma + 1)s = 23.3 \tag{3}$$

The numerical solutions computed with 25 PPW are shown in Fig. 4, from which it is found that the first coalescence time is $t_c^* = 23.3$. This numerical result exactly equals the theoretical result obtained by Eq. (3). A series of shocks is gradually combined to one N wave, which has a long wavelength and low amplitude, and this wave is maintained until it dies down, as shown in Fig. 4.

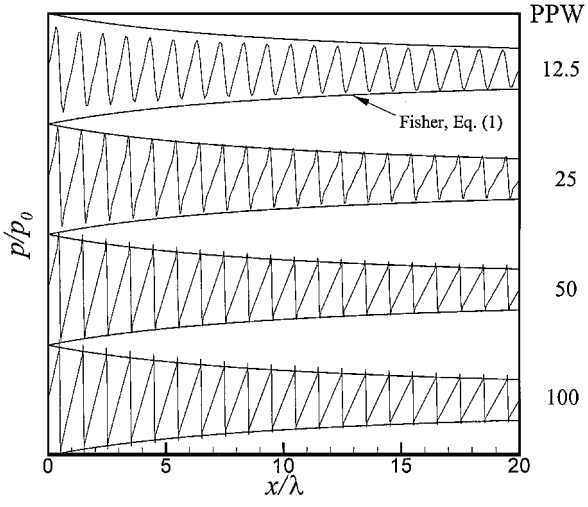


**Fig. 3 Numerical simulation of regular N-wave propagation.**

## Conclusions

The propagation of the nonlinear N wave is well simulated by using the techniques of CAA. The optimized high-order compact finite difference schemes, the ANAD model, and the characteristic boundary conditions are effectively used to produce time-accurate solutions. To resolve the N-wave characteristics, it is found that at least 25 grid points are required per wavelength. The numerical results of regular and irregular N-wave propagation show good agreement with previous theoretical analyses. Thus, CAA methodology may be applicable to prediction of the MPT noise propagation, and it is expected that more practical problems can be studied intensively, including three-dimensional effects and open-end ducts.

## References

[1]Hawkings, D., "Multiple Tone Generation by Transonic Compressors," *Journal of Sound and Vibration*, Vol. 17, No. 2, 1971, pp. 241–250.

[2]Kurosaka, M., "A Note on Multiple Pure Tone Noise," *Journal of Sound and Vibration*, Vol. 19, No. 4, 1971, pp. 453–462.

[3]Fisher, M. J., Tester, B. J., and Schwaller, P. J. G., "Supersonic Fan Tone Noise Prediction," *Proceedings of the 4th AIAA/CEAS Aeroacoustics Conference*, AIAA, Reston, VA, 1998, pp. 290–300.

[4]McApline, A., and Fisher, M. J., "On the Prediction of 'Buzz-Saw' Noise in Aero-Engine Inlet Ducts," *Journal of Sound and Vibration*, Vol. 248, No. 1, 2001, pp. 123–149.

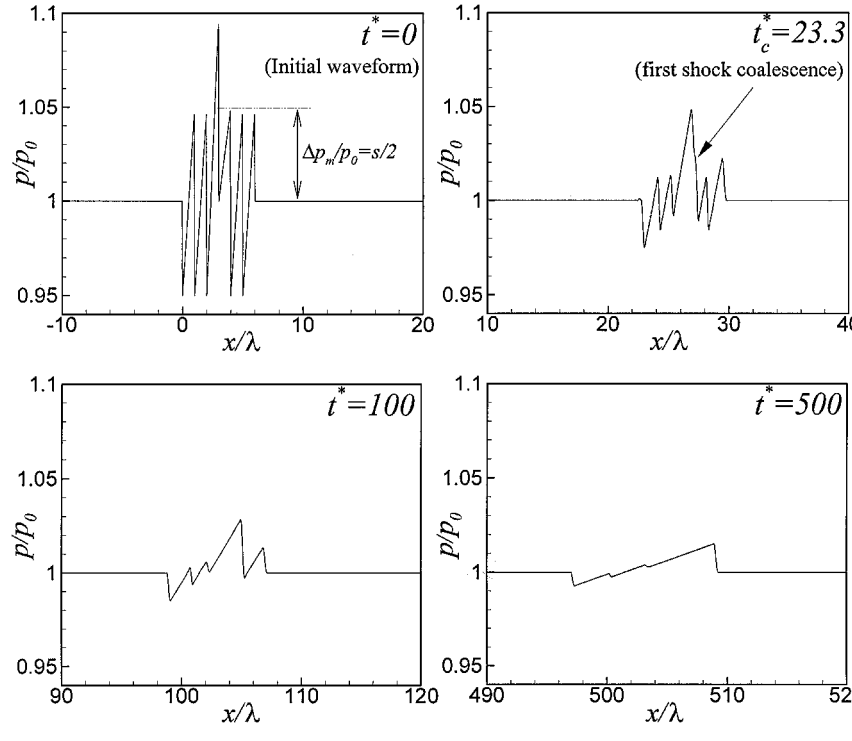


**Fig. 4 Numerical simulation of irregular N-wave propagation.**

[5]Kim, J. W., and Lee, D. J., "Optimized Compact Finite Difference Schemes with Maximum Resolution," *AIAA Journal*, Vol. 34, No. 5, 1996, pp. 887–893.

[6]Kim, J. W., and Lee, D. J., "Adaptive Nonlinear Artificial Dissipation Model for Computational Aeroacoustics," *AIAA Journal*, Vol. 39, No. 5, 2001, pp. 810–818.

[7]Whitham, G. B., *Linear and Nonlinear Waves*, Wiley, New York, 1974.

[8]Thomson, K. W., "Time Dependent Boundary Conditions for Hyperbolic Systems," *Journal of Computational Physics*, Vol. 68, No. 1, 1987, pp. 1–24.

W. J. Devenport
*Associate Editor*

# Effects of Combustion on the Sound Pressure Generated by Circular Jet Flows

Kapil K. Singh,* Steven H. Frankel,† and Jay P. Gore‡
*Purdue University, West Lafayette, Indiana 47907-1003*

## Introduction

MANY studies of the sound generated by premixed turbulent jet flames are available in the literature.[1–7] Some studies of the sound generated by nonpremixed turbulent flames with a coflow of air also exist.[1,4,8,9] Experimental data also exist for sound emitted by a coflow partially premixed flame[10] and by industrial burner flames.[11] Efforts have been made to correlate the sound generation of the flames to various flow properties and flame parameters. Price et al.[1] correlated sound generated by turbulent premixed and diffusion flames with the changes in the intensity of light emission by free radicals. Giammar and Putnam[2] presented sound pressure level data as a function of the square of the firing rate and also as a function of the product of pressure drop and heat release rate. Kilham and Kirmani[5] showed that combustion noise increased with turbulence intensity in premixed jet flames. Kotake and Takamoto[6,7] investigated the effects of the shape and the size of the burner nozzle on the combustion noise of premixed flames. They also investigated the effects of the turbulence in the unburned mixture on the acoustic characteristics. Ohiwa et al.[8] studied the relationship between flame structure and noise characteristics for coflow nonpremixed turbulent flames. They were able to show that fluctuations in sound pressure, ion current, temperature, and CH emission corresponded to organized eddy formation.

Shivashankara et al.[3] compared flame-generated noise for premixed turbulent flames with the corresponding cold-jet noise. They showed that the sound generated by the premixed flames differs from that generated by the cold jets in terms of scaling, directionality, and spectral content. Kumar[4] studied the sound generated by both premixed and coflow nonpremixed turbulent flames and found significant differences in their characteristics. Recently, for a nonreacting jet, Narayanan et al.[12] found a downstream low-frequency source ($5 \le x/D \le 10$) and an upstream high-frequency source ($0 \le x/D \le 3$). The contributions from farther downstream ($x/D \ge 10$) were found to be small. The data for heated jets indicated that the sources are distributed farther downstream compared to those in the cold jets. Narayanan et al.[12] showed that for a fixed exit velocity a cold jet is noisier than the corresponding heated jet. The present work involves jets that are at much lower exit Mach numbers compared to those studied by Narayanan et al.[12] The acoustic characteristics of the present low-Mach-number jets and flames are of interest in combustion instability studies, where acoustic fluctuations of the low-Mach-number jets serve as the perturbations that can grow by coupling with the combustor modes.

The specific objectives of the present work are to obtain sound pressure level (SPL) data for turbulent nonpremixed flames, with fuel issuing into quiescent surrounding air. Review of literature shows that sound generation phenomena from this simple configuration of nonpremixed combustion have not been studied in detail. Past studies of sound generation from nonpremixed flames involved a wide range of burner dimensions with a coflow, a pilot flame, or a flame holder. None of the past measurements are for flames for which detailed velocity, temperature, and species concentration statistics, necessary for a description of the aerothermo-acoustic phenomena, are available. A complete set of measurements including velocity and scalar statistics, in addition to the sound pressure measurements, is necessary for validation of aeroacoustic and thermoacoustic computational models. We have selected two turbulent nonpremixed flame (TNF) workshop standard flames, German Aerospace Center DLR-A and DLR-B, because of the availability of the extensive experimental data for velocities, species concentrations, and thermal radiation properties[13,14] (also private communication from A. Dreizler, 2000), as well as the simplicity of the configuration. The SPL produced by the flames are compared with those produced by nonreacting air jets with identical exit Reynolds numbers *Re*. Note that the Mach number *M* rather than the Reynolds number *Re* is the appropriate nondimensional parameter for studies of aeroacoustics. However, for identical tube diameters, the exit velocity and the exit Mach number are linearly proportional to the exit Reynolds number. Therefore, the Reynolds number, which is the appropriate parameter for studying inertial and diffusive effects and turbulence, is used simply as the designator of the jets in the present study. SPL measurements were also performed for four flames (for which velocity and scalar field data do not exist) and corresponding six air jets to study the velocity and exit Mach number scaling.

## Experimental Arrangement

TNF standard flames DLR-A and DLR-B were stabilized in the laboratory. The fuel stream of these flames contains $CH_4$, 22.1%; $H_2$, 33.2%; and $N_2$, 44.7% by mole. The flames were stabilized on a standard 0.8-cm-internal-diameter burner with a sharp exit. The exit Reynolds numbers for the two flames based on injected gas properties at room temperature are $1.52 \times 10^4$ (DLR-A) and $2.28 \times 10^4$ (DLR-B). Air was used for studying the sound emission from equivalent nonreacting jets with the same burner. The flow in each case has very low exit Mach numbers ($M = 0.04$–$0.18$) based on the sound speed at room temperature. The three fuel stream constituents were supplied from bottled sources and measured using calibrated sonic orifices. A pipe length of more than $500L/D$ ensured proper mixing before the flow reached the burner exit. The burner was placed with its exit 76 cm above the floor, firing vertically upward and 160 cm away from the nearest wall. Acoustic measurements were made using a Realistic Sound Level Meter (Model 33-2050). The SPL was read in terms of A-weighted decibels (dBA referenced to 0.0002 $\mu$bar) and recorded using a National Instrument ADC board and a personal computer. The meter has an accuracy of $\pm 2$ dB at 114 dB. This meter was checked using a B&K 4230 sound level calibrator producing 94 dB at 1 kHz and also with a B&K 4231 sound level meter producing 94 dB and 114 dB SPL at 1 kHz. The Realistic Sound Level Meter returned accurate measurements in all cases, well within 2 dB. The maximum spherical solid angle for the sound level meter in present measurements, with the assumption that the sources are distributed along the full observed length of flames, is about 71.5 deg. As per the manufacturer's catalog, the sound level meter has less than 2-dB systematic variations in directional sensitivity for frequencies less than 8 kHz within this spherical solid angle. Spectral measurements show that for the flows considered here most of the energy is below 8 kHz, limiting the effects of

Received 20 May 2002; revision received 17 September 2002; accepted for publication 17 September 2002. 

*Doctoral Student, School of Mechanical Engineering. Member AIAA.
†Associate Professor, School of Mechanical Engineering. Member AIAA.
‡Vincent P. Reilly Professor, School of Mechanical Engineering; gore@ecn.purdue.edu. Associate Fellow AIAA.